

Turning in the landscape: a new mechanism for generating Primordial Black Holes

Jacopo Fumagalli, Sébastien Renaux-Petel, John W. Ronayne and Lukas T. Witkowski
*Institut d'Astrophysique de Paris, GReCO, UMR 7095 du CNRS et
de Sorbonne Université, 98bis boulevard Arago, Paris 75014, France*
(Dated: May 8, 2020)

We propose a new model-independent mechanism for producing Primordial Black Holes from a period of multi-field inflation. The required enhancement of primordial fluctuations compared to their value at CMB scales naturally occurs when the inflationary trajectory in the landscape exhibits a limited period of strongly non-geodesic motion. Such trajectories with multiple dynamical fields are motivated by the search for ultraviolet completions of inflation. We study analytically and numerically how the parameters describing the bending impact the primordial fluctuations power spectrum and the mass function of Primordial Black Holes. Our mechanism has the potential of exhibiting unique features accessible to observation through its Primordial Black Hole spectrum and stochastic background of gravitational waves, offering a precious glimpse at the dynamics of inflation in the landscape.

Introduction.— The nature of Dark Matter (DM) is a great riddle of contemporary fundamental physics. A possibility that has been entertained for some time is that all or a fraction of DM can consist of Primordial Black Holes (PBHs) [1], i.e. black holes resulting from the collapse of local overdensities in the early universe. The idea that quantum fluctuations during cosmological inflation are responsible for seeding the overdensities responsible for PBH creation has been contemplated since the early work of [2–4]. A particular challenge is that the amplitude of fluctuations needs to be larger by a factor of $\sim 10^7$ compared to the amplitude observed at CMB scales $\mathcal{P} \sim 10^{-9}$ to lead to a significant production of PBHs. In models of single-field inflation this can be achieved by invoking suitable features in the single field Lagrangian [5–14] or by coupling the inflation to gauge fields [15–17]. An enhancement of fluctuations can also be triggered in the waterfall phase in hybrid inflation [3, 18–21].

In this letter, we present a new PBH production mechanism specific to multi-field inflationary scenarios and with potentially unique observational signatures. Motivated by embeddings of inflation in high-energy physics, a promising arena for inflationary model-building involves trajectories characterized by strongly non-geodesic motion [22–35]. In this context we show that a limited phase of strongly non-geodesic motion can enhance the curvature fluctuation power spectrum sufficiently to allow for subsequent PBH formation. The effect is not restricted to a particular realization of inflation. To highlight this, the background evolution will be described by the time-dependence of the Hubble scale H and of the quantity η_\perp characterizing the bending of the inflationary trajectory in field space. The height, width and position of the peak in the power spectrum are determined by the amplitude of η_\perp and the time where bending occurs, as we show numerically and analytically using the tools from [27, 36–38], finding in particular that the growth of the power spectrum can overcome the bound deduced in the single-field case [39–41]. We further analyze how the model parameters affect the mass spectrum of PBHs assuming

Gaussian statistics for the fluctuations.

Inflationary models with strongly non-geodesic motion exhibit a characteristic pattern of non-Gaussianity (NG), with a bispectrum and higher-order correlation functions enhanced for flattened configurations [36, 37, 42]. Given the inherent sensitivity of the PBH abundance on departures from Gaussian statistics (see [43–51]), this offers the exciting prospect of characteristic features in the PBH spectrum. In addition, the NG may also lead to a tell-tale signal in the stochastic background of gravitational waves (GWs) produced non-linearly at horizon re-entry of the scalar fluctuations [52–54], which is potentially observable in near-future GW observatories [55–64]. A detection of such features would offer invaluable insights into the dynamics behind inflation.

Multi-field dynamics and strong bending.— Our starting point is the generic two-derivative action for two scalar fields ϕ^I minimally coupled to gravity:

$$S = \int d^4x \sqrt{-g} \left[\frac{M_{\text{Pl}}^2}{2} R - \frac{1}{2} G_{IJ} \nabla^\mu \phi^I \nabla_\mu \phi^J - V(\phi) \right], \quad (1)$$

where $G_{IJ}(\phi)$ defines a metric in the internal field space parametrized by the coordinates ϕ^I . The inflationary background dynamics is characterized by a spatially flat Friedmann-Lemaître-Robertson-Walker metric with scale factor $a(t)$, Hubble parameter $H(t) = \dot{a}/a$, and homogeneous scalar fields whose equations of motion read $\mathcal{D}_t \dot{\phi}^I + 3H \dot{\phi}^I + G^{IJ} V_{,J} = 0$, where the time field-space covariant derivative of any field space vector A^I is defined as $\mathcal{D}_t A^I = \dot{A}^I + \Gamma_{JK}^I \dot{\phi}^J A^K$. For later convenience we define $\dot{\sigma} \equiv (G_{IJ} \dot{\phi}^I \dot{\phi}^J)^{1/2}$ and $\epsilon \equiv -\dot{H}/H^2$. It is particularly useful to introduce the adiabatic-entropic basis defined by $e_\sigma^I \equiv \dot{\phi}^I / \dot{\sigma}$ and e_s^I , which is orthogonal to e_σ^I , and with a definite orientation for the basis (e_σ^I, e_s^I) . The latter evolve as

$$\mathcal{D}_t e_\sigma^I = H \eta_\perp e_s^I, \quad \mathcal{D}_t e_s^I = -H \eta_\perp e_\sigma^I, \quad (2)$$

where the dimensionless “bending” parameter η_\perp measures the deviation of the background trajectory from a field-space geodesic [65, 66].

To describe the physics of scalar linear fluctuations about the above background, we work in the comoving gauge, with $\delta\phi^I = Q_s e_s^I$ and the spatial part of the metric reading $g_{ij} = a^2 e^{2\zeta} \delta_{ij}$. The so-called comoving curvature perturbation ζ is ultimately the quantity of direct observational interest, while Q_s embodies the genuine multi-field effects. The quadratic action governing their dynamics can be cast in the simple form [66–68] (writing $S = \int dt d^3x \mathcal{L}$)

$$\mathcal{L}^{(2)} = a^3 \left[M_{\text{Pl}}^2 \epsilon \left(\dot{\zeta}^2 - \frac{(\partial\zeta)^2}{a^2} \right) + 2\dot{\sigma}\eta_{\perp} \dot{\zeta} Q_s + \frac{1}{2} \left(\dot{Q}_s^2 - \frac{(\partial Q_s)^2}{a^2} - m_s^2 Q_s^2 \right) \right], \quad (3)$$

where the entropic mass reads

$$m_s^2 = V_{;ss} - H^2 \eta_{\perp}^2 + \epsilon H^2 M_{\text{Pl}}^2 R_{\text{fs}}, \quad (4)$$

with $V_{;ss} = e_s^I e_s^J V_{;IJ}$ the projection of the covariant Hessian of the potential along the entropic direction, and R_{fs} the field space scalar curvature.

Motivated by the search for ultraviolet completions of inflation, a lot of attention has recently been dedicated to inflationary backgrounds characterized by strongly non-geodesic motion, with $\eta_{\perp}^2 \gg 1$ [22–35]. Instrumental to our mechanism is the fact that a strong bending can naturally result in a large and negative m_s^2/H^2 , signaling an instability of entropic fluctuations for $k^2/a^2 \lesssim |m_s^2|$. Through the kinetic coupling provided by the same bending, such an instability is transferred to the curvature perturbation, resulting in its exponential growth compared to a standard setup. On general grounds, one can deduce from (3) that on super-Hubble scales, the curvature perturbation is sourced by the entropic fluctuations, $\dot{\zeta} = -2H^2 \eta_{\perp} / \dot{\sigma} Q_s$, but that the entropic fluctuations evolves independently, $\ddot{Q}_s + 3H\dot{Q}_s + m_{s,(\text{eff})}^2 Q_s = 0$, with an effective super-Hubble mass $m_{s,(\text{eff})}^2 = m_s^2 + 4\eta_{\perp}^2 H^2$ to which the bending contributes positively. In situations with strong bending, the tachyonic instability mentioned above is therefore transient, with the large and positive $m_{s,(\text{eff})}^2/H^2$ indicating a stable background, and resulting in a rapid super-Hubble decay of Q_s , as well as the large-scale conservation of the curvature perturbation. The properties of the latter can be understood in terms of the single-field effective field theory of inflation, valid after entropic mass crossing, but with an unusual imaginary sound speed $c_s^2 = m_s^2/m_{s,(\text{eff})}^2 < 0$, allowing one to efficiently characterize the enhancement of higher-order correlation functions in flattened configurations [27, 36–38]. As for the power spectrum, it is exponentially amplified compared to the single-field prediction $\mathcal{P}_0 = H^2/(8\pi^2 \epsilon M_{\text{Pl}}^2)_{k=aH}$, with [38]

$$\mathcal{P}_{\zeta} = \mathcal{P}_0 e^{2x}, \quad x = \frac{\pi}{2} \left(2 - \sqrt{3 + \xi} \right) \eta_{\perp}, \quad (5)$$

where $\xi < 1$ such that $m_s^2/H^2 = \eta_{\perp}^2 (\xi - 1)$ being related to the Hessian and geometrical contributions to m_s^2 .

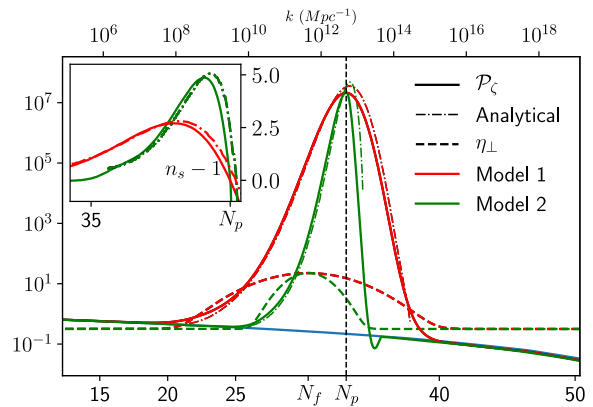


FIG. 1. Power spectra for the two models discussed in the text compared to their bending profiles. The dot-dashed curves represent the analytical approximation in Eq. (8). The blue line corresponds to the single-field power spectrum \mathcal{P}_0 for the same $H(N)$. Here and in other figures, power spectra are normalized to one at the CMB pivot scale.

PBH generation mechanism.— Suppose that the inflationary trajectory approximately follows a geodesic when the CMB scales exit the Hubble radius, and then exhibits strong bending before relaxing back to a geodesic. From the properties summarized above one then expects an exponential enhancement of the power spectrum for the scales exiting the Hubble radius around the feature, while leaving the other scales almost unaffected. In order to study this mechanism independently of any precise microscopic realization, let us highlight that the quadratic action (3) shows that the physics of linear fluctuations of any two-field model can be described by only three functions of the number of e -folds $N = \ln(a)$: the Hubble scale $H(N)$, like in single-field models, the entropic mass $m_s^2(N)$, and the bending $\eta_{\perp}(N)$. In the following, we use this effective approach to focus on the main characteristics of our proposal.¹ We assume that $H(N)$ is featureless, and consider a simple Gaussian profile for the bending

$$\eta_{\perp} = \eta_{\perp}^{\max} e^{-\frac{(N-N_f)^2}{2\Delta^2}}. \quad (6)$$

Here, N_f and Δ set respectively the time and duration of the feature. As for the entropic mass, we write $m_s^2/H^2 = b - \eta_{\perp}^2$, where we consider b constant for simplicity, concentrating on the time variation of m_s^2 set by the bending itself. In the numerical examples below, we will consider two benchmark models characterized respectively by $(\Delta^2, \eta_{\perp}^{\max}) = (10, 22.53)$ and $(2, 22.9)$, with $b = 1$, $N_f = 30.3$ after Hubble exit of the CMB pivot scale, and $H(N)$ corresponding to Starobinsky inflation (see the discussion after Eq. (13) for the rationale behind

¹ Concrete UV realizations of our mechanism may exhibit further features, making its phenomenology even richer.

these numbers). The non-negligible value of b , expected on general grounds [69, 70], implies that modes exiting the Hubble radius before the feature go through it unaffected. Indeed, it ensures that the corresponding entropic fluctuations have decayed by the time of the feature, and therefore ζ is conserved.

In fig. 1 the solid lines show the numerically computed power spectra for the two models above, together with the corresponding evolutions of $\eta_{\perp}(N)$. This plot shows the effectiveness of our mechanism to boost the small scale power spectrum by a large factor of $\sim 10^7$ compared to CMB scales, as required for a significant production of PBHs. There, we also display the result of an analytical approximation, which provides a good fit and enables one to understand the mechanisms behind the specific shapes of the power spectra. To appreciate this, let us note that the dynamics of each k -mode is characterized by two times, \tilde{N} corresponding to entropic mass crossing and the onset of the instability, and \bar{N} corresponding to the effective sound horizon crossing where ζ becomes constant:

$$\frac{k}{a(\tilde{N})} = |m_s(\tilde{N})|, \quad \& \quad \frac{k|c_s|}{a(\bar{N})} = H(\bar{N}), \quad (7)$$

(in our limit where $(\eta_{\perp}^{\max})^2 \gg b$, $|c_s|^{-1} \simeq \sqrt{3}$). Hence, the result (5) for the power spectrum can be used in our context if the quantity $x(N)$ there can be considered approximately constant between \tilde{N} and \bar{N} , i.e. $(\bar{N} - N_f)^2 - (\tilde{N} - N_f)^2 \lesssim 4\Delta^2$, in which case one can write

$$\mathcal{P}_{\zeta}(k) = \mathcal{P}_0(k)e^{2x}|_{\tilde{N}_k}, \quad (8)$$

for each k mode that satisfies $k/a(\tilde{N}_k) = |m_s|$ when $m_s^2 < 0$, and where the evaluation at \tilde{N}_k is motivated by the fact that most of the growth occurs at early times. One expects this approximation to underestimate the power spectrum before the peak, as η_{\perp} grows in the interval $[\tilde{N}, \bar{N}]$ for those modes, and to overestimate it after the peak for opposite reasons. This is indeed what we observe in fig. 1, but this does not prevent our approximation to provide relevant information as we now show.²

Characteristics of the peak.— From the analytical approximation (8), one deduces that the mode k_p corresponding to the peak of the power spectrum is the one whose entropic mass crossing coincides with the peak of η_{\perp} , i.e. $\tilde{N}_{k_p} = N_f$, and hence

$$k_p \simeq k_f ((\eta_{\perp}^{\max})^2 - b)^{1/2}, \quad (9)$$

where k_f is the scale that exits the Hubble radius at N_f . The corresponding height of the peak is given by

$$\gamma \equiv \ln \left(\frac{\mathcal{P}}{\mathcal{P}_0} \right) \Big|_{\text{peak}} = \pi(2 - \sqrt{3 + b/(\eta_{\perp}^{\max})^2}) \eta_{\perp}^{\max}. \quad (10)$$

² For the mode with $\tilde{N} = N_f$, the criterion for the validity of the approximation reads $(4\Delta^2)^{-1} \ln^2(|c_s|\eta_{\perp}^{\max}) \lesssim 1$, with the left-hand side given by 0.1 and 0.7 for Model 1 and 2 respectively.

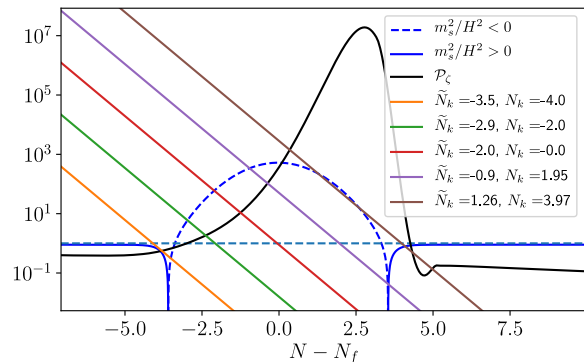


FIG. 2. Family of lines $k^2/(aH)^2$ equally $\ln k$ -divided, i.e. $\delta N \simeq 2$, for modes whose entropic mass crossing happens while $m_s^2 < 0$ for Model 2. More modes enter the region of instability before the parameter $|m_s^2|/H^2$ has passed its peak than after, resulting in an asymmetric peak for the power spectrum despite a symmetric profile for $|m_s^2|/H^2$.

As the abundance of PBHs is highly sensitive to the precise amplitude of fluctuations, we warn that this relation is only approximate. Keeping this in mind, note that for $(\eta_{\perp}^{\max})^2 \gg b$ one has $k_p/k_f \simeq \gamma/c$ with $c = \pi(2 - \sqrt{3})$, relating the location of the feature, the location of the peak, and the maximal enhancement of the power spectrum. The modes that are enhanced are the ones whose entropic mass crossing happens while $m_s^2 < 0$. From fig. 2, it is hence easy to understand the asymmetry of the peak, as a larger range of modes enjoys this characteristic before the peak of $|m_s|$ than afterwards. As for the largest mode k_e to be enhanced, it is the one whose line $k^2/(aH)^2$ is tangent to m_s^2/H^2 in fig. 2, corresponding to $\tilde{N}_e \simeq N_f + \Delta^2$. To estimate the growth rate of the power spectrum, one can compute the spectral index from (8):

$$(n_s - 1) - (n_s - 1)_0 = K \frac{d\eta_{\perp}}{d\tilde{N}} \left(1 + \frac{d \ln \eta_{\perp}}{d\tilde{N}} \frac{1}{(1 - b/\eta_{\perp}^2)} \right)^{-1} \\ \simeq c \frac{N_f - \tilde{N}}{\Delta^2 + N_f - \tilde{N}} \eta_{\perp}, \quad (11)$$

where $K = \pi(2 - 3(3 + b/\eta_{\perp}^2)^{-1/2})$ and all quantities on the left hand side are evaluated at time \tilde{N}_k . The first line is valid for any time-dependence of $\eta_{\perp}(N)$, while the second is specific to our Gaussian profile with $(\eta_{\perp}^{\max})^2 \gg b$. The apparent divergence for $(\tilde{N} - N_f) \rightarrow \Delta^2$ is not problematic, as the analytical approximation is not valid close to the mode k_e that last gets enhanced. More importantly, Eq. (11) shows that the stronger and/or the sharper the bending, the steeper the peak of the power spectrum (within the regime of validity of the analytical approximation). While not surprising by itself, it is interesting that it can easily overcome the bound for n_s found in single-field inflation [39–41]. The very good agreement between the analytical formula for n_s and the numerical

result is shown in fig. 1, where one can see for instance that $n_s - 1$ reaches 5 in the model with a sharper bending.

PBH spectrum.— The main quantity of interest is the mass spectrum $f(M)$, which is related to the fraction of DM in PBHs through $\Omega_{\text{PBH}} = \Omega_{\text{CDM}} \int f(M) d \ln M$. An important ingredient in its calculation is the probability density function (PDF) for the smoothed density contrast δ [71, 72], with a high sensitivity of the PBH abundance to the tail of the PDF [43–51]. Although a derivation of the PDF is beyond the scope of this work, we provide tentative results for the mass function by assuming Gaussian statistics. In this case $f(M)$ is given by [73, 74]:

$$f(M) = \frac{2}{\Omega_{\text{CDM}}} \int_{-\infty}^{\infty} \frac{M}{\gamma M_H} \mu^{1/\gamma} \sqrt{\frac{M_{H,\text{eq}}}{M_H}} \times \frac{1}{\sqrt{2\pi\sigma^2(M_H)}} \exp\left(-\frac{(\mu^{1/\gamma} + \delta_c)^2}{2\sigma^2(M_H)}\right) d \ln M_H, \quad (12)$$

where we defined $\mu \equiv M/(C M_H)$ and $C = 3.3$, $\gamma = 0.36$, $\delta_c = 0.45$ are numerical parameters whose values are taken from simulations of PBH formation [73, 75–78], assuming critical collapse [79–82]. Here, $\sigma(M_H)$ is the variance of the power spectrum of the smoothed density contrast, which can be computed as

$$\sigma^2(k) = \left(\frac{4}{9}\right)^2 \int_0^{\infty} \frac{dq}{q} (qk^{-1})^4 e^{-q^2/k^2} \mathcal{P}_\zeta(q), \quad (13)$$

where we assumed radiation domination during PBH formation and used a Gaussian window function for the smoothing. To relate the comoving scale k of a mode re-entering the horizon to the corresponding Hubble volume mass M_H we evolve these quantities from their respective values at matter-radiation equality, where they are known, using $k = k_{\text{eq}} \sqrt{M_{H,\text{eq}}/M_H}$ with $k_{\text{eq}} = 0.01 (\Omega_m/0.31) \text{ Mpc}^{-1}$ and $M_{H,\text{eq}} \approx 2.8 \times 10^{17} M_\odot$. This combined with (9) leads to the interesting relation $M_{H,\text{feat}} \simeq (\eta_\perp^{\text{max}})^2 M_{H,\text{peak}}$ that links the position of the feature, the size of the bending and the peak of the mass distribution.

In fig. 3 we plot $f(M)$ for the benchmark models introduced above. The model parameters have been chosen purposefully such that PBHs constitute all of DM at matter-radiation equality, i.e. $\Omega_{\text{PBH}}/\Omega_{\text{CDM}} = \int_{-\infty}^{\infty} f(M) d \ln M = 1$, and so that $f(M)$ peaks near $M_{\text{PBH}} \sim 10^{-13} M_\odot$, which lies in the window where PBH can constitute a significant fraction of DM [83]. We refrain from directly comparing $f(M)$ against observational constraints, as these constraints are typically derived for monochromatic PBH spectra, while we have a non-monochromatic mass spectrum, for which the constraints would need to be reprocessed [84]. The mass function $f(M)$ is sensitive to the shape of the power spectrum [85]. Here we observe that a steeper growth of the power spectrum corresponding to a larger value of n_s results in a narrower peak for $f(M)$.

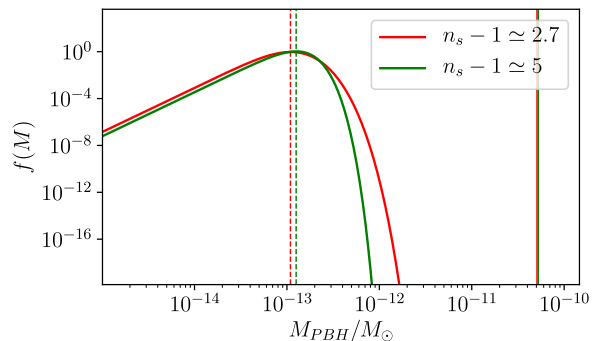


FIG. 3. PBH mass spectrum $f(M)$ for the two benchmark models, corresponding to $n_s - 1 = 2.7, 5$. The dashed lines indicate the location of the peak of $f(M)$. The solid lines on the RHS denote the horizon mass at re-entry of the scale corresponding to maximal bending.

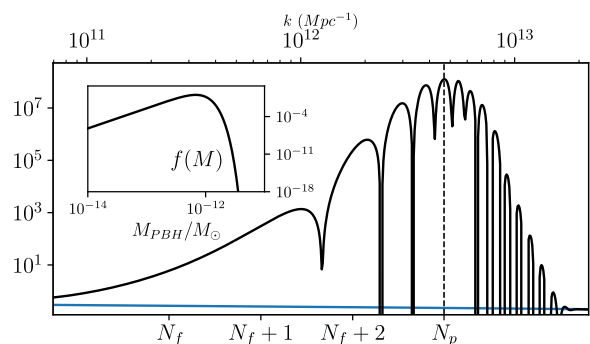


FIG. 4. For sharper bending ($\eta_\perp^{\text{max}} = 68$, $\Delta^2 = 0.1$) the shape of the power spectrum exhibits characteristic oscillatory patterns. These oscillations do not translate into features of the PBH mass distribution, at least with the assumption of a Gaussian PDF.

In the case of sharper turns our analytical methods do not apply, but the power spectrum can still be computed numerically. In fig. 4 we display \mathcal{P}_ζ for a model with ($\Delta^2 = 0.1, \eta_\perp^{\text{max}} = 68$), which exhibits oscillatory patterns characteristic of sharp turns (see e.g. [86, 87]). The mass function $f(M)$ for this model is free of oscillations, as a consequence of the two integrations involved in (12) and (13). Thus, patterns in the correlation functions seem to be washed out when Gaussian statistics is considered and probing these distinctive features would require to go beyond this approximation.

Discussion.— Modern embeddings of inflation in high energy physics suggest that inflation may be of multi-field type. In this context we observe that periods of strongly non-geodesic motion produce enhancements in the scalar power spectrum \mathcal{P}_ζ which are sufficient to trigger subsequent production of PBHs. We show that the position, amplitude and shape of the peak in \mathcal{P}_ζ depend on the details of the non-geodesic motion in a precise and quantifiable way.

The mechanism presented has the potential of exhibit-

ing several unique features accessible to observation. One such characteristic signal arises from the sensitivity of the PBH abundance on the probability distribution, as observed in the study of the impact of primordial NGs [43–51].³ Inflationary trajectories with strongly non-geodesic motion exhibit a characteristic pattern of NG, with a bispectrum and higher-order correlation functions enhanced for flattened configurations [36, 37, 42]. This type of NG differs from that whose effect on the PBH abundance has been considered so far and may manifest itself in a distinct feature in $f(M)$.

Another pathway for experimental scrutiny of our mechanism is via its GW signal. GWs are sourced during the phase of inflation, but also through anisotropic stresses during the re-entry of scalar fluctuations [52–54], carrying information about the inflationary dynamics (see e.g. [55–57]). Thus, the characteristic features

inherent to the presented mechanism lead to the exciting prospect of an observational fingerprint potentially detectable with LISA and other near-future GW observatories [58–64].

Note added.— While this work was being finalized, a similar idea appeared in [88] with a focus on a complementary parametric regime. Our main results agree.

ACKNOWLEDGMENTS

We are grateful to Sebastian Garcia-Saenz, Shi Pi, Lucas Pinol, Caner Ünal and Vincent Vennin for interesting and helpful discussions. J.F, S.RP, J.W.R and L.T.W are supported by the European Research Council under the European Union’s Horizon 2020 research and innovation programme (grant agreement No 758792, project GEODESI).

-
- [1] G. F. Chapline, *Nature* **253**, 251 (1975).
 [2] P. Ivanov, P. Naselsky, and I. Novikov, *Phys. Rev. D* **50**, 7173 (1994).
 [3] J. Garcia-Bellido, A. D. Linde, and D. Wands, *Phys. Rev. D* **54**, 6040 (1996), arXiv:astro-ph/9605094 [astro-ph].
 [4] J. S. Bullock and J. R. Primack, *Phys. Rev. D* **55**, 7423 (1997), arXiv:astro-ph/9611106.
 [5] K. Kohri, D. H. Lyth, and A. Melchiorri, *JCAP* **0804**, 038 (2008), arXiv:0711.5006 [hep-ph].
 [6] M. Kawasaki, A. Kusenko, Y. Tada, and T. T. Yanagida, *Phys. Rev. D* **94**, 083523 (2016), arXiv:1606.07631 [astro-ph.CO].
 [7] J. Garcia-Bellido and E. Ruiz Morales, *Phys. Dark Univ.* **18**, 47 (2017), arXiv:1702.03901 [astro-ph.CO].
 [8] C. Germani and T. Prokopec, *Phys. Dark Univ.* **18**, 6 (2017), arXiv:1706.04226 [astro-ph.CO].
 [9] H. Motohashi and W. Hu, *Phys. Rev. D* **96**, 063503 (2017), arXiv:1706.06784 [astro-ph.CO].
 [10] G. Ballesteros and M. Taoso, *Phys. Rev. D* **97**, 023501 (2018), arXiv:1709.05565 [hep-ph].
 [11] M. P. Hertzberg and M. Yamada, *Phys. Rev. D* **97**, 083509 (2018), arXiv:1712.09750 [astro-ph.CO].
 [12] Y.-F. Cai, X. Tong, D.-G. Wang, and S.-F. Yan, *Phys. Rev. Lett.* **121**, 081306 (2018), arXiv:1805.03639 [astro-ph.CO].
 [13] G. Ballesteros, J. Beltran Jimenez, and M. Pieroni, *JCAP* **06**, 016 (2019), arXiv:1811.03065 [astro-ph.CO].
 [14] R.-G. Cai, Z.-K. Guo, J. Liu, L. Liu, and X.-Y. Yang, (2019), arXiv:1912.10437 [astro-ph.CO].
 [15] A. Linde, S. Mooij, and E. Pajer, *Phys. Rev. D* **87**, 103506 (2013), arXiv:1212.1693 [hep-th].
 [16] E. Bugaev and P. Klimai, *Phys. Rev. D* **90**, 103501 (2014), arXiv:1312.7435 [astro-ph.CO].
 [17] V. Domcke, F. Muia, M. Pieroni, and L. T. Witkowski, *JCAP* **1707**, 048 (2017), arXiv:1704.03464 [astro-ph.CO].
 [18] D. H. Lyth, (2011), arXiv:1107.1681 [astro-ph.CO].
 [19] E. Bugaev and P. Klimai, *Phys. Rev. D* **85**, 103504 (2012), arXiv:1112.5601 [astro-ph.CO].
 [20] S. Clesse and J. Garcia-Bellido, *Phys. Rev. D* **92**, 023524 (2015), arXiv:1501.07565 [astro-ph.CO].
 [21] M. Kawasaki and Y. Tada, *JCAP* **1608**, 041 (2016), arXiv:1512.03515 [astro-ph.CO].
 [22] S. Renaux-Petel and K. Turzyński, *Phys. Rev. Lett.* **117**, 141301 (2016), arXiv:1510.01281 [astro-ph.CO].
 [23] A. Achcarro, V. Atal, C. Germani, and G. A. Palma, *JCAP* **02**, 013 (2017), arXiv:1607.08609 [astro-ph.CO].
 [24] A. R. Brown, *Phys. Rev. Lett.* **121**, 251601 (2018), arXiv:1705.03023 [hep-th].
 [25] S. Mizuno and S. Mukohyama, *Phys. Rev. D* **96**, 103533 (2017), arXiv:1707.05125 [hep-th].
 [26] P. Christodoulidis, D. Roest, and E. I. Sfakianakis, *JCAP* **11**, 002 (2019), arXiv:1803.09841 [hep-th].
 [27] S. Garcia-Saenz, S. Renaux-Petel, and J. Ronayne, *JCAP* **1807**, 057 (2018), arXiv:1804.11279 [astro-ph.CO].
 [28] A. Achúcarro and G. A. Palma, *JCAP* **1902**, 041 (2019), arXiv:1807.04390 [hep-th].
 [29] T. Bjorkmo and M. C. D. Marsh, *JHEP* **04**, 172 (2019), arXiv:1901.08603 [hep-th].
 [30] T. Bjorkmo, *Phys. Rev. Lett.* **122**, 251301 (2019), arXiv:1902.10529 [hep-th].
 [31] P. Christodoulidis, D. Roest, and E. I. Sfakianakis, *JCAP* **12**, 059 (2019), arXiv:1903.06116 [hep-th].
 [32] V. Aragam, S. Paban, and R. Rosati, (2019), arXiv:1905.07495 [hep-th].
 [33] R. Bravo, G. A. Palma, and S. Riquelme, *JCAP* **02**, 004 (2020), arXiv:1906.05772 [hep-th].
 [34] S. Garcia-Saenz, L. Pinol, and S. Renaux-Petel, *JHEP* **01**, 073 (2020), arXiv:1907.10403 [hep-th].
 [35] D. Chakraborty, R. Chiovoloni, O. Loaiza-Brito, G. Niz, and I. Zavala, *JCAP* **01**, 020 (2020), arXiv:1908.09797 [hep-th].
 [36] S. Garcia-Saenz and S. Renaux-Petel, *JCAP* **11**, 005

³ The nonlinear relation between δ and ζ also gives intrinsic NG statistics for the density contrast [47].

- (2018), arXiv:1805.12563 [hep-th].
- [37] J. Fumagalli, S. Garcia-Saenz, L. Pinol, S. Renaux-Petel, and J. Ronayne, Phys. Rev. Lett. **123**, 201302 (2019), arXiv:1902.03221 [hep-th].
- [38] T. Bjorkmo, R. Z. Ferreira, and M. C. D. Marsh, JCAP **1912**, 036 (2019), arXiv:1908.11316 [hep-th].
- [39] C. T. Byrnes, P. S. Cole, and S. P. Patil, JCAP **06**, 028 (2019), arXiv:1811.11158 [astro-ph.CO].
- [40] P. Carrilho, K. A. Malik, and D. J. Mulryne, Phys. Rev. D **100**, 103529 (2019), arXiv:1907.05237 [astro-ph.CO].
- [41] O. zsoy and G. Tasinato, (2019), arXiv:1912.01061 [astro-ph.CO].
- [42] R. Z. Ferreira, (2020), arXiv:2003.13410 [astro-ph.CO].
- [43] C. T. Byrnes, E. J. Copeland, and A. M. Green, Phys. Rev. **D86**, 043512 (2012), arXiv:1206.4188 [astro-ph.CO].
- [44] S. Young and C. T. Byrnes, JCAP **08**, 052 (2013), arXiv:1307.4995 [astro-ph.CO].
- [45] G. Franciolini, A. Kehagias, S. Matarrese, and A. Riotto, JCAP **03**, 016 (2018), arXiv:1801.09415 [astro-ph.CO].
- [46] V. Atal and C. Germani, Phys. Dark Univ. **24**, 100275 (2019), arXiv:1811.07857 [astro-ph.CO].
- [47] V. De Luca, G. Franciolini, A. Kehagias, M. Peloso, A. Riotto, and C. nal, JCAP **07**, 048 (2019), arXiv:1904.00970 [astro-ph.CO].
- [48] G. Panagopoulos and E. Silverstein, (2019), arXiv:1906.02827 [hep-th].
- [49] C.-M. Yoo, J.-O. Gong, and S. Yokoyama, JCAP **09**, 033 (2019), arXiv:1906.06790 [astro-ph.CO].
- [50] V. Atal, J. Cid, A. Escrivà, and J. Garriga, (2019), arXiv:1908.11357 [astro-ph.CO].
- [51] J. M. Ezquiaga, J. García-Bellido, and V. Vennin, (2019), arXiv:1912.05399 [astro-ph.CO].
- [52] S. Mollerach, D. Harari, and S. Matarrese, Phys. Rev. D **69**, 063002 (2004), arXiv:astro-ph/0310711.
- [53] K. N. Ananda, C. Clarkson, and D. Wands, Phys. Rev. D **75**, 123518 (2007), arXiv:gr-qc/0612013.
- [54] D. Baumann, P. J. Steinhardt, K. Takahashi, and K. Ichiki, Phys. Rev. D **76**, 084019 (2007), arXiv:hep-th/0703290.
- [55] J. Garcia-Bellido, M. Peloso, and C. Unal, JCAP **12**, 031 (2016), arXiv:1610.03763 [astro-ph.CO].
- [56] K. Inomata, M. Kawasaki, K. Mukaida, Y. Tada, and T. T. Yanagida, Phys. Rev. D **95**, 123510 (2017), arXiv:1611.06130 [astro-ph.CO].
- [57] J. Garcia-Bellido, M. Peloso, and C. Unal, JCAP **09**, 013 (2017), arXiv:1707.02441 [astro-ph.CO].
- [58] S. Kuroyanagi, T. Chiba, and T. Takahashi, JCAP **11**, 038 (2018), arXiv:1807.00786 [astro-ph.CO].
- [59] R.-g. Cai, S. Pi, and M. Sasaki, Phys. Rev. Lett. **122**, 201101 (2019), arXiv:1810.11000 [astro-ph.CO].
- [60] N. Bartolo, V. De Luca, G. Franciolini, A. Lewis, M. Peloso, and A. Riotto, Phys. Rev. Lett. **122**, 211301 (2019), arXiv:1810.12218 [astro-ph.CO].
- [61] N. Bartolo, V. De Luca, G. Franciolini, M. Peloso, D. Racco, and A. Riotto, Phys. Rev. D **99**, 103521 (2019), arXiv:1810.12224 [astro-ph.CO].
- [62] R.-G. Cai, S. Pi, S.-J. Wang, and X.-Y. Yang, JCAP **05**, 013 (2019), arXiv:1901.10152 [astro-ph.CO].
- [63] C. Caprini, D. G. Figueroa, R. Flauger, G. Nardini, M. Peloso, M. Pieroni, A. Ricciardone, and G. Tasinato, JCAP **11**, 017 (2019), arXiv:1906.09244 [astro-ph.CO].
- [64] E. Barausse *et al.*, (2020), 10.1007/s10714-020-02691-1., arXiv:2001.09793 [gr-qc].
- [65] S. Groot Nibbelink and B. van Tent, (2000), arXiv:hep-ph/0011325.
- [66] S. Groot Nibbelink and B. van Tent, Class. Quant. Grav. **19**, 613 (2002), arXiv:hep-ph/0107272.
- [67] M. Sasaki and E. D. Stewart, Prog. Theor. Phys. **95**, 71 (1996), arXiv:astro-ph/9507001.
- [68] D. Langlois and S. Renaux-Petel, JCAP **04**, 017 (2008), arXiv:0801.1085 [hep-th].
- [69] X. Chen and Y. Wang, Phys. Rev. D **81**, 063511 (2010), arXiv:0909.0496 [astro-ph.CO].
- [70] X. Chen and Y. Wang, JCAP **04**, 027 (2010), arXiv:0911.3380 [hep-th].
- [71] S. Young, C. T. Byrnes, and M. Sasaki, JCAP **1407**, 045 (2014), arXiv:1405.7023 [gr-qc].
- [72] S. Young, Int. J. Mod. Phys. **D29**, 2030002 (2019), arXiv:1905.01230 [astro-ph.CO].
- [73] J. C. Niemeyer and K. Jedamzik, Phys. Rev. Lett. **80**, 5481 (1998), arXiv:astro-ph/9709072 [astro-ph].
- [74] C. T. Byrnes, M. Hindmarsh, S. Young, and M. R. S. Hawkins, JCAP **1808**, 041 (2018), arXiv:1801.06138 [astro-ph.CO].
- [75] J. C. Niemeyer and K. Jedamzik, Phys. Rev. **D59**, 124013 (1999), arXiv:astro-ph/9901292 [astro-ph].
- [76] I. Musco, J. C. Miller, and L. Rezzolla, Class. Quant. Grav. **22**, 1405 (2005), arXiv:gr-qc/0412063 [gr-qc].
- [77] I. Musco, J. C. Miller, and A. G. Polnarev, Class. Quant. Grav. **26**, 235001 (2009), arXiv:0811.1452 [gr-qc].
- [78] I. Musco and J. C. Miller, Class. Quant. Grav. **30**, 145009 (2013), arXiv:1201.2379 [gr-qc].
- [79] M. W. Choptuik, Phys. Rev. Lett. **70**, 9 (1993).
- [80] T. Koike, T. Hara, and S. Adachi, Phys. Rev. Lett. **74**, 5170 (1995), arXiv:gr-qc/9503007 [gr-qc].
- [81] C. Gundlach, Living Rev. Rel. **2**, 4 (1999), arXiv:gr-qc/0001046 [gr-qc].
- [82] C. Gundlach, Phys. Rept. **376**, 339 (2003), arXiv:gr-qc/0210101 [gr-qc].
- [83] B. Carr, K. Kohri, Y. Sendouda, and J. Yokoyama, (2020), arXiv:2002.12778 [astro-ph.CO].
- [84] B. Carr, M. Raidal, T. Tenkanen, V. Vaskonen, and H. Veermäe, Phys. Rev. **D96**, 023514 (2017), arXiv:1705.05567 [astro-ph.CO].
- [85] C. Germani and I. Musco, Phys. Rev. Lett. **122**, 141302 (2019), arXiv:1805.04087 [astro-ph.CO].
- [86] A. Achúcarro, J.-O. Gong, S. Hardeman, G. A. Palma, and S. P. Patil, JCAP **01**, 030 (2011), arXiv:1010.3693 [hep-ph].
- [87] J. Chluba, J. Hamann, and S. P. Patil, Int. J. Mod. Phys. D **24**, 1530023 (2015), arXiv:1505.01834 [astro-ph.CO].
- [88] G. A. Palma, S. Sypsas, and C. Zenteno, (2020), arXiv:2004.06106 [astro-ph.CO].